


Article

A Label-Free Electrochemical Aptasensor Based on Zn/Fe Bimetallic MOF Derived Nanoporous Carbon for Ultra-Sensitive and Selective Determination of Paraquat in Vegetables

Qiaoling Wu ^{1,2,*} , Han Tao ^{1,2,*}, Yuangen Wu ^{1,2}, Xiao Wang ^{1,2}, Qili Shi ^{1,2} and Donglin Xiang ^{1,2}¹ School of Liquor and Food Engineering, Guizhou University, Guiyang 550025, China² Key Laboratory of Fermentation Engineering and Biopharmacy of Guizhou Province, Guizhou University, Guiyang 550025, China

* Correspondence: htiao@gzu.edu.cn; Tel.: +86-0851-88236895

Abstract: Paraquat (PQ) has high acute toxicity, even at low concentrations. For most people, the main pathway of exposure to PQ is through the diet. Therefore, the development of simple and efficient methods for PQ testing is critical for ensuring food safety. In this study, a new electrochemical detection strategy for paraquat is proposed based on the specific binding of PQ to its nucleic acid aptamer. Firstly, the Zn/Fe bimetallic ZIF derived nanoporous carbon (Zn/Fe-ZIF-NPC) and nickel hexacyanoferrate nanoparticles (NiHCF-NPs) were sequentially modified onto the glassy carbon electrode (GCE). NiHCF-NPs served as the signal probes, while Zn/Fe-ZIF-NPC facilitated electron transfer and effectively enhanced the sensing signal of NiHCF-NPs. Au nanoparticles (AuNPs) were then electrodeposited on the NiHCF-NPs/Zn/Fe-ZIF-NPC/GCE and then the thiolated aptamer was assembled on the AuNPs/NiHCF-NPs/Zn/Fe-ZIF-NPC/GCE via Au-S bonding. When incubated with PQ, the formation of PQ-aptamer complexes delayed the interfacial electron transport reaction of NiHCF-NPs, which caused a decrease in the current signals. As a result, simple and highly sensitive detection of PQ can be readily achieved by detecting the signal changes. A linear range was obtained from 0.001 to 100 mg/L with a detection limit as low as 0.34 µg/L. Due to the recognition specificity of the aptamer to its target molecule, the proposed method has excellent anti-interference ability. The prepared electrochemical aptasensor was successfully used for PQ assay in lettuce, cabbage and agriculture irrigation water samples with recoveries ranging from 96.20% to 104.02%, demonstrating the validity and practicality of the proposed method for PQ detection in real samples.



Citation: Wu, Q.; Tao, H.; Wu, Y.; Wang, X.; Shi, Q.; Xiang, D. A Label-Free Electrochemical Aptasensor Based on Zn/Fe Bimetallic MOF Derived Nanoporous Carbon for Ultra-Sensitive and Selective Determination of Paraquat in Vegetables. *Foods* **2022**, *11*, 2405. <https://doi.org/10.3390/foods11162405>

Academic Editor: Thierry Noguer

Received: 22 June 2022

Accepted: 8 August 2022

Published: 10 August 2022

Publisher's Note: MDPI stays neutral with regard to jurisdictional claims in published maps and institutional affiliations.



Copyright: © 2022 by the authors. Licensee MDPI, Basel, Switzerland. This article is an open access article distributed under the terms and conditions of the Creative Commons Attribution (CC BY) license (<https://creativecommons.org/licenses/by/4.0/>).

Keywords: paraquat; Zn/Fe bimetallic MOF; nanoporous carbon; electrochemical aptasensor; label-free; food safety

1. Introduction

Food safety has always been a global issue of great concern. Among the various food hazards, the adverse effects caused by excessive pesticide residues in food cannot be neglected. The abuse of pesticides not only causes environmental pollution, but also poses a serious threat to public health.

Paraquat (PQ), 1,1-dimethyl-4,4-bipyridine dichloride, is one of the most widely used herbicides [1] in the world because of its low cost and nonselective features. However, paraquat is highly toxic and can cause severe damage to vital organs such as the lung and liver [2,3], as well as inducing cancer and weakening immunity [4]. As a result, the EU has banned PQ since 2007 and has listed PQ in the database of compounds that should be monitored in food samples [5]. China has also banned the use of PQ since July 2016, but illegal use of paraquat still occurs frequently and therefore the maximum residue limits (MRLs) for PQ in different foods are still regulated in the latest Chinese food safety

standards (GB 2763-2021). Moreover, more than 90 countries worldwide still allow the use or limited use of PQ [6–8]. However, due to its chemical stability and solubility in water, PQ can easily accumulate in the environment and in agricultural products, and then enter the human body via food chain. PQ contamination in agricultural products is one of the highly concerning food safety issues in many countries [9]. It has been reported that PQ was detected in various food products including cabbage, guava, eggplant and round gourd [10,11]. Therefore, the development of rapid and accurate PQ detection methods is essential for the timely protection of consumer health.

In the past, efforts and achievements have been made for PQ detection by employing Liquid Chromatography (LC) [12], Gas Chromatography-Mass Spectrometry (GC-MS) [13], Surface enhanced Raman spectroscopy (SERS) [14], etc. However, expensive instruments, time-consuming pre-processing steps and specialized operations do not allow for the low cost, simple and fast detection of PQ, so new detection methods still need to be developed. Electroanalysis technology has become a promising food safety testing technique due to its low cost, high sensitivity and simple operation [15,16]. For PQ assay, the currently reported electrochemical method is basically based on direct reduction of PQ [17,18]. However, when the sample matrix is complex, coexisting species which can also be reduced near the PQ reduction potential will seriously interfere with PQ determination, i.e., there is a deficiency of low detection specificity.

Aptamers are monomeric DNA or RNA oligonucleotide molecules that are chemically synthesized *in vitro* and can bind target molecules with high specificity [19,20], and have been widely used in biosensors as a new generation of biometric molecules [21]. Inspired by this, we considered that the combination of PQ aptamer with electrochemical sensing could achieve high specificity detection of PQ. It is exciting that the PQ aptamer has been successfully obtained by our group with the Capture-SELEX technique [22].

To achieve high sensitivity PQ detection simultaneously, the electrochemical sensing signal needs to be effectively improved, and the simplest way is to modify the electrodes with functional materials. Metal organic framework (MOF) materials, a new category of nanoporous substances, are crystalline porous coordination polymers formed by assembling metal ions or metal clusters with organic ligands [23]. The organic ligands in MOFs contain a large amount of carbon, thus the nanoporous carbon (NPC) materials can be obtained by direct carbonization of MOFs. In contrast to inorganic porous materials (e.g., molecular sieves), NPC has a large specific surface area, rich pore architecture, high stability and electrical conductivity, which can effectively promote electron transfer [24], and is often used as a heterogeneous catalyst to improve the catalytic activity of different electrode reactions [25]. Moreover, NPC also has good biocompatibility [26]. Therefore, it can be used as an ideal material for modifying electrodes with a view to improving the performance of the electrodes.

Herein, we propose a new label-free electrochemical aptasensor that can be used for the determination of PQ in vegetables with high specificity and sensitivity. The sensing interface was designed using NiHCF-NPs, immobilized directly on the working electrode as redox probes to produce sensing signals, thus overcoming the disadvantage of needing to label electroactive substances on the aptamer or target molecule. Zn/Fe-ZIF-NPC modified on GCE acted as an electrocatalyst to improve the electrochemical signal produced by NiHCF-NPs. Subsequently, AuNPs were electrodeposited on the NiHCF-NPs/Zn/Fe-ZIF-NPC/GCE. The deposited AuNPs not only bound the aptamer to the GCE surface, but also greatly increased the sensing signals. After the PQ molecules in test solution were bound to the Apt/AuNPs/NiHCF-NPs/Zn/Fe-ZIF-NPC/GCE via the affinity of aptamer, the change of current signal was measured and used as the quantitative indicator to achieve a simple, reliable and highly sensitive detection of PQ. To the best of our knowledge, although three aptamer-based PQ detection methods have been reported [22,27,28], they are all based on the colorimetric technique. So far, electrochemical aptasensors for PQ detection have not been reported yet.

2. Experimental Section

2.1. Apparatus and Reagents

Apparatus: Scanning electron microscopy (SEM) observations were made with SUPRA 40 microscope (ZEISS, Germany). N₂ adsorption/desorption measurements (77.3 K) were performed using the Micromeritics ASAP2020 sorptometer (Micromeritics, USA). Atomic Force Microscopy (AFM) observation was done with a Dimension FastScan (Bruker, Germany). Electrochemical experiments were conducted on a CHI660e electrochemical workstation (CH Instrument Company, China). A GCE (3 mm diameter) was taken as working electrode, while an Ag/AgCl electrode and a Pt electrode were taken as reference and counter electrode, respectively.

Reagents: Zn(NO₃)₂·6H₂O, FeSO₄·7H₂O, NH₄OH, 2-Methylimidazole, K₃[Fe(CN)₆], K₄[Fe(CN)₆], HAuCl₄, PQ, Tris-HCl buffer, 6-mercapto-1-hexanol (MCH), Tris(2-carboxyethyl) phosphine Hydrochloride(TCEP), methanol and ethanol were obtained from Aladdin Chemical (Shanghai, China). KCl, NiCl₂, Na₂HPO₄, NaH₂PO₄ were purchased from Macklin reagent corporation (Shanghai, China). The thiolated PQ-15 sequence was synthesized by Sangon Biotech. Co., Ltd. (Shanghai, China): 5'-sh-(CH₂)₆-ACC GAC CGT GCT GGA CTC TCG CGC AGC GCC GAG TCC GAA CTG GGT GGG GAG TAT GAG CGA GCG TTG CG-3'.

2.2. Screening for PQ Aptamer

Aptamer of PQ (PQ-15) was screened *in vitro* by Capture-SELEX technique according to literature [22]. The biotin-labeled auxiliary primer P3 (5'-Biotin-CGCAACGCTCGC-3') was paired with the 3'-end of a random single-stranded oligonucleotide library (5'-ACCGACCGTGCTGGACTCT-N30-AGTATGAGCGAGCGTTGCG-3') by base complementing, and subsequently immobilized on streptavidin-modified magnetic beads. Then, different concentrations of PQ solutions (500–50 μM) were incubated with magnetic beads and the ssDNA with PQ specific affinity was obtained after elution, which was subjected to asymmetric PCR amplification and purification of the product to obtain a secondary ssDNA library for the next round of screening. After 9 rounds of SELEX screening, the collected PQ affinity sequences were cloned for sequencing, then 15 ssDNA sequences with PQ affinity were obtained. The 15 ssDNA sequences were subjected to homology analysis and secondary structure prediction, and then 6 ssDNA sequences were screened and their dissociation constants (K_d) were calculated, and finally the PQ-15 sequence with the highest affinity for paraquat was selected.

2.3. Synthesis of Zn/Fe-ZIF-NPC

According to previous literature [29], Zn/Fe bimetallic zeolite type MOF (Zn/Fe-ZIF) was first synthesized as follows: The solution A was obtained by weighing 21.27 g of Zn(NO₃)₂·6H₂O and 0.994 g of FeSO₄·7H₂O into a flask containing 100 mL of methanol and stirring continuously until completely dissolved. Solution B was obtained by adding 3.75 g of 2-methylimidazole to 100 mL of methanol and stirring until completely dissolved. Solution A and solution B were mixed and stirred to react at room temperature for 24 h. Following centrifugation at 10,000 rpm for 10 min, the sediment was washed several times with methanol and subsequently dried at 50 °C under vacuum to give Zn/Fe-ZIF. Next, 1 g of Zn/Fe-ZIF was added into the mixture of 10 mL furfuryl alcohol and 1 mL ammonium hydroxide and stirred overnight. The product was then washed, dried and transferred to a tube furnace and heated at 80 °C under N₂ protection for 24 h, then held at 150 °C for 6 h and finally heated to 900 °C at 2 °C min⁻¹ for 2 h. The resulting solid was washed with ethanol and ultrapure water and freeze-dried to give Zn/Fe-ZIF-NPC. To modify GCE, Zn/Fe-ZIF-NPC dispersion (1 mg/mL) was prepared by dispersing 2 mg of Zn/Fe-ZIF-NPC in 2 mL of water/isopropyl alcohol/0.1 wt% nafion (volume ratio 7.8:2.0:0.2). Zn/Fe-ZIF dispersion (1 mg/mL) was obtained in the same way.

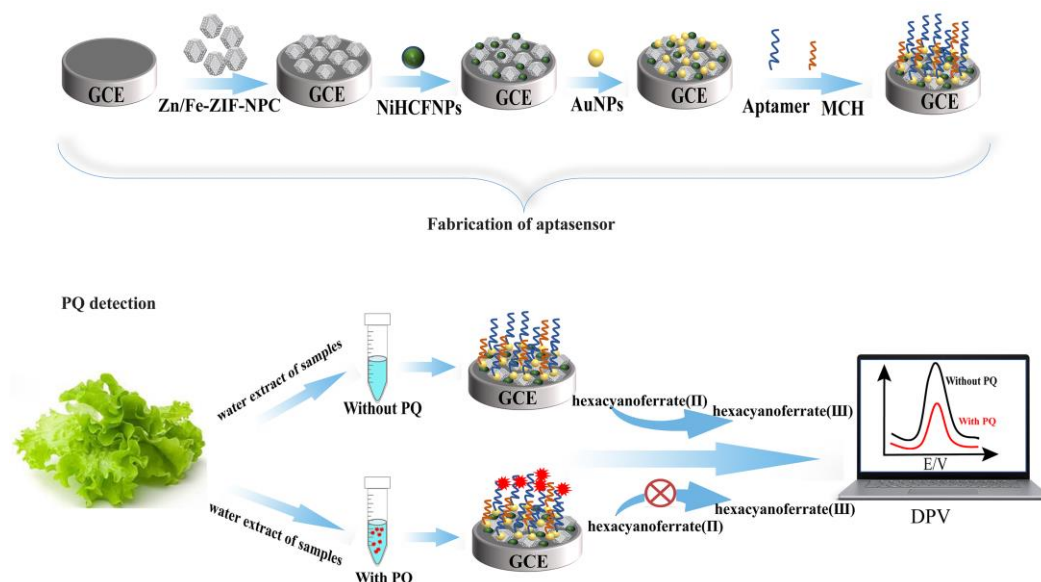
2.4. Synthesis of NiHCF-NPs

NiHCF-NPs were obtained according to literature [30]. At first, 70 mL of 0.01 mol/L NiCl₂ solution was added drop by drop into 70 mL of 0.05 mol/L K₃[Fe(CN)₆] solution containing 0.05 mol/L KCl, and vigorous stirring was continued for 5 min. The solution was then immediately centrifuged and the solid fraction was collected and washed three times with ultrapure water. Finally, the solids were vacuum dried at 40 °C for 12 h to give yellow NiHCF-NPs. NiHCF-NPs were dispersed in water to produce a 1 mg/mL dispersion, which was stored at 4 °C prior to use.

2.5. Fabrication of Aptasensor

Briefly, the GCE surface was polished with Al₂O₃ power (0.05 μm) and ultrasonically cleaned with ethanol and water. Then, 8 μL of Zn/Fe-ZIF-NPC solution was dropped on GCE surface and dried at room temperature. Subsequently, 6 μL of NiHCF-NPs solution was coated on the Zn/Fe-ZIF-NPC/GCE. After thorough drying, the NiHCF-NPs/Zn/Fe-ZIF-NPC/GCE were placed in 1 mM HAuCl₄ containing 0.1 M KCl and 50 mM H₂SO₄, where AuNPs were electrodeposited on the NiHCF-NPs/Zn/Fe-ZIF-NPC/GCE by 12 cyclic voltametric scans over 0~+1.0 V range at a scan rate of 50 mV s⁻¹. The modified GCE was denoted as AuNPs/NiHCF-NPs/Zn/Fe-ZIF-NPC/GCE.

Prior to immobilization, 20 μM of aptamer was mixed with 2 mM TCEP to reduce disulfide bonds in the aptamer, and then heated at 95 °C for 5 min with a constant temperature metal bath. Next, it was placed in a refrigerator at 4 °C for 15 min. The aptamer concentration was then diluted to 2.5 μM with 20 mM Tris-HCl buffer (pH 7.0). Subsequently, the AuNPs/NiHCF-NPs/Zn/Fe-ZIF-NPC/GCE was incubated with 2.5 μM of aptamer at 4 °C for 12 h to bind the aptamer to the working electrode via Au-S bonds. Finally, 6 μL of 1 mM MCH was placed on the modified working electrode to block non-specific adsorption at room temperature for 40 min and the resulting working electrode was labelled as MCH/Apt/AuNPs/NiHCF-NPs/Zn/Fe-ZIF-NPC/GCE. The fabrication procedure is shown in Scheme 1.



Scheme 1. Illustration of the aptasensor fabrication process and PQ detection.

2.6. Electrochemical Measurement and PQ Detection

Cyclic voltammetry (CV) and electrochemical impedance spectroscopy (EIS) were used to characterize the preparation process of the aptasensor. CV experiments were performed in 0.1 M PBS (pH 7.0) from $-0.1\sim 0.8$ V at the scan rate of 50 mV s⁻¹. EIS experiments were performed in 0.1 M KCl solution containing a 5 mM [Fe(CN)₆]^{3-/4-} (1:1)

mixture with a voltage frequency range of 0.01 Hz to 10 kHz, and the electron transfer resistance (R_{et}) was calculated based on Randles equivalent circuit to evaluate the electron transfer ability of different modified GCEs. For PQ detection, aptasensors were incubated with test solutions containing different concentrations of PQ for 60 min, washed carefully with 0.1 M PBS and then immersed in 0.1 M PBS (pH 7.0) to record the current responses by differential pulse voltammetry (DPV). The percentage drop in current signal (ΦI) was calculated according to the following formula:

$$\Phi I(\%) = (I_0 - I_1) / I_0 \times 100$$

where I_0 and I_1 represent the peak current before and after incubation with PQ, respectively. In DPV experiments, the pulse amplitude was 0.05 V, the pulse width was 0.05 s and the pulse period was 0.5 s. The stability, reproducibility and interference tests of the sensors were also investigated by DPV.

2.7. Real Samples Preparation

Vegetables and river water (irrigation water) located at vegetable growing areas were selected as actual samples. Cabbage and lettuce samples were obtained from farmers in Huaxi District, Guiyang City, China. Sample preparation was conducted referring to previous literature [31]. Fresh lettuce and cabbage were cut into small pieces, respectively. Then, 20 g samples were homogenized with 50 mL water in a stirrer for 5 min and the mixture was then sonicated for 1 h. After filtration through a 0.22 μm membrane, the filtrate collected was used as the test samples. Water samples were taken from the Huaxi River (26°44'36" N, 106°67'82" E), which is used as irrigation water for farmland. Prior to testing, the water sample was first centrifuged to remove solid particles, and then the supernatant was filtered through a 0.22 μm membrane and used as the test sample directly. For recovery experiments, the above test samples were spiked with PQ standard solution to configure samples with different PQ concentrations.

3. Results

3.1. Characterization of Nanomaterials

The surface morphology of Zn/Fe-ZIF and Zn/Fe-ZIF-NPC were characterized using SEM. Figure 1A shows Zn/Fe-ZIF has a rhombic dodecahedral structure with a diameter of approximately 700 nm. After carbonization, the obtained Zn/Fe-ZIF-NPC still retains the rhombic dodecahedral structure of Zn/Fe-ZIF precursor (Figure 1B). The morphology of NiHCF-NPs was shown in Figure 1C. It can be seen that the prepared NiHCF-NPs have a diameter of about 20–40 nm. Figure 1D is the SEM image of electrodeposited AuNPs. It can be observed that the gold particles are evenly distributed with a diameter of about 30 nm.

The specific surface area and pore size distribution of Zn/Fe-ZIF-NPC were investigated by nitrogen adsorption/desorption experiments carried out at 77.3 K. As displayed in Figure 2A, the nitrogen adsorption/desorption isotherms of Zn/Fe-ZIF-NPC were type IV with a conspicuous H2-type hysteresis loop, indicating that Zn/Fe-ZIF-NPC has high porosity. The pore size distribution curves (Figure 2B) illustrate that the Zn/Fe-ZIF-NPC possesses a hierarchical porous structure with micropores and mesopores. Besides, the Brunauer–Emmett–Teller (BET) surface area of Zn/Fe-ZIF-NPC was calculated as 401.66 $\text{m}^2 \text{g}^{-1}$. The high specific surface area and porosity make Zn/Fe-ZIF-NPC possess good absorbability, which is conducive to the immobilization of NiHCF-NPs redox probe.

Besides, electrochemical AC impedance spectroscopy were recorded to compare the interface properties of Zn/Fe-ZIF/GCE, Zn/Fe-ZIF-NPC/GCE and bare GCE in 0.1 M KCl solution containing 5 mM $[\text{Fe}(\text{CN})_6]^{3-/4-}$ (1:1). Fitted the Nyquist plots in Figure 2C with Randles Equivalent circuit, the electron transfer resistance (R_{et}) for different GCEs was: Zn/Fe-ZIF/GCE (1245 Ω) > bare GCE (692 Ω) > Zn/Fe-ZIF-NPC/GCE (445 Ω). Compared with Zn/Fe-ZIF/GCE and bare GCE, Zn/Fe-ZIF-NPC/GCE has lower electron transfer resistance, indicating that Zn/Fe-ZIF-NPC can effectively accelerate the electron transfer

at the electrode interface, which is undoubtedly beneficial for improving the sensing performance of the aptasensor.

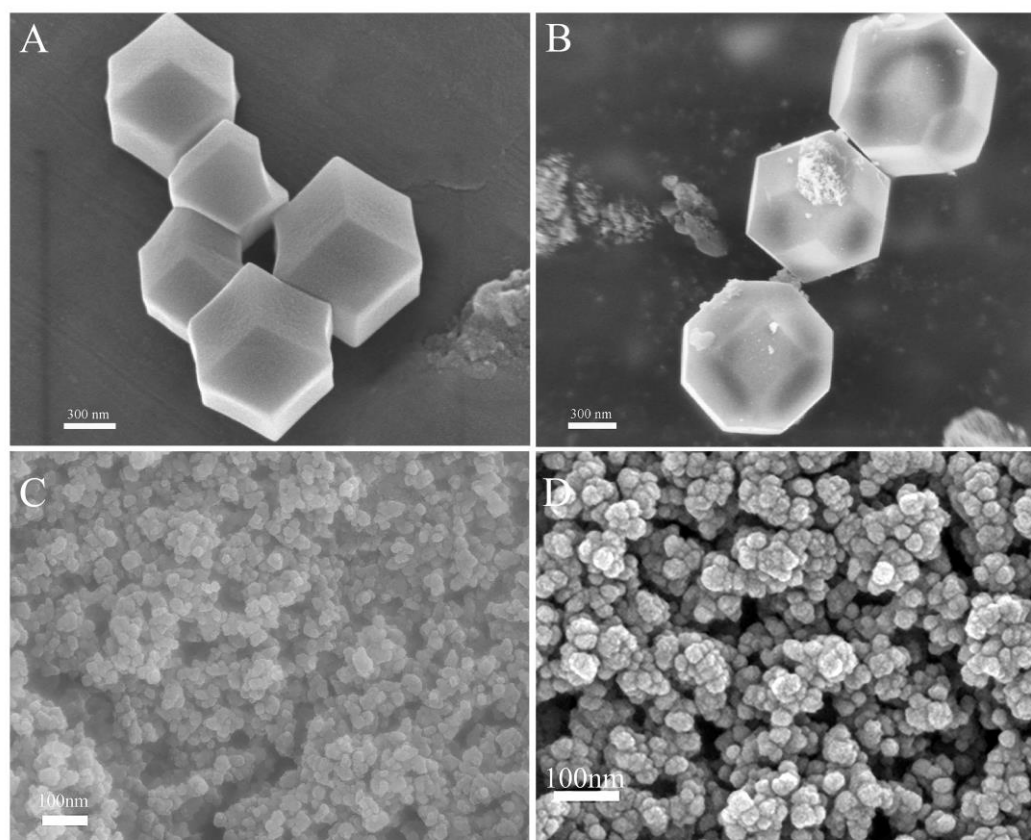


Figure 1. SEM images of Zn/Fe-ZIF (A), Zn/Fe-ZIF-NPC (B), NiHCF-NPs (C) and AuNPs (D).

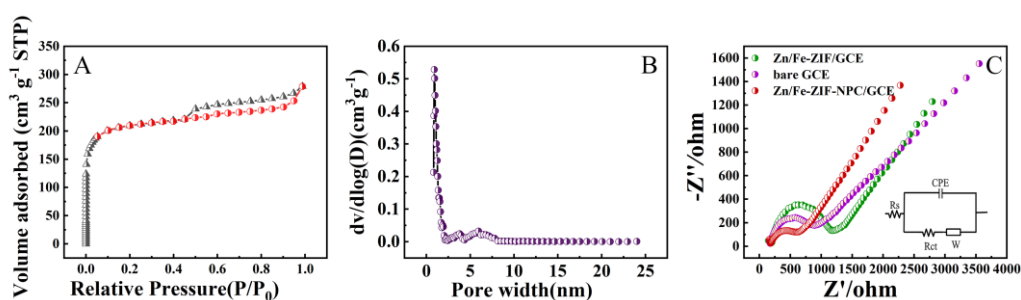


Figure 2. (A) N₂ adsorption/desorption isotherms of Zn/Fe-ZIF-NPC, (B) Pore size distributions of Zn/Fe-ZIF-NPC, (C) EIS of bare GCE, Zn/Fe-ZIF/GCE and Zn/Fe-ZIF-NPC/GCE in 0.1 M KCl (containing 5 mM [Fe(CN)₆]^{3-/4-}). Zn/Fe-ZIF loading volume: 8 μ L; Zn/Fe-ZIF-NPC loading volume: 8 μ L.

3.2. Characterization of Modified GCEs

The elemental composition of the AuNPs/NiHCF-NPs/Zn/Fe-ZIF-NPC/GCE surface was determined by EDS. As displayed in Figure 3, Au, Ni, Fe, Zn, C and O elements were found on the AuNPs/NiHCF-NPs/Zn/Fe-ZIF-NPC/GCE surface, and these six elements were highly dispersed on the modified GCE's surface, indicating that the modification materials were successfully immobilized on the GCE surface.

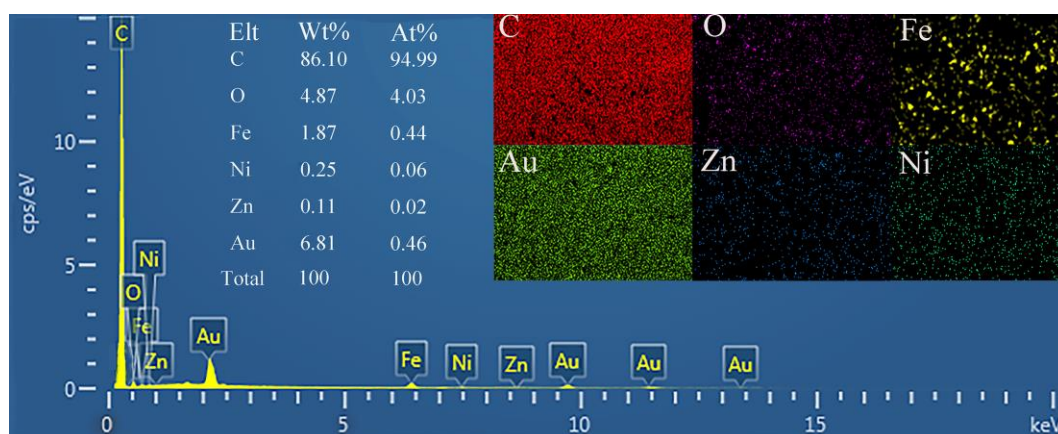


Figure 3. EDS spectrum of AuNPs/NiHCF-NPs/Zn/Fe-ZIF-NPC/GCE. Zn/Fe-ZIF loading volume: 8 μ L; Zn/Fe-ZIF-NPC loading volume: 8 μ L. CV cycle number of AuNPs electrodeposition: 10.

The surfaces of AuNPs/NiHCF-NPs/Zn/Fe-ZIF-NPC/GCE and Apt/AuNPs/NiHCF-NPs/Zn/Fe-ZIF-NPC/GCE were observed by atomic force microscopy (AFM). As shown in Figure 4, the GCE surface became rougher after the bond of aptamer. The surface roughness was calculated from the AFM height images using root-mean-square value (RMS) and surface area difference. The surface height of AuNPs/NiHCF-NPs/Zn/Fe-ZIF-NPC/GCE was obtained as 388.8 nm with an RMS of approximately 33.26 nm, while the surface height of Apt/AuNPs/NiHCF-NPs/Zn/Fe-ZIF-NPC/GCE increased to 412.2 nm and the surface roughness increased to 50.37 nm, which indicates that aptamers were effectively immobilized on the AuNPs/NiHCF-NPs/Zn/Fe-ZIF-NPC/GCE surface.

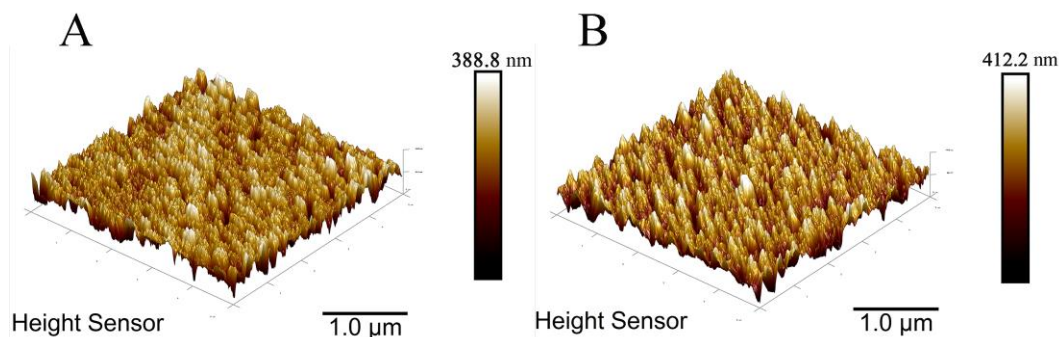


Figure 4. AFM images of AuNPs/NiHCF-NPs/Zn/Fe-ZIF-NPC/GCE (A) and Apt/AuNPs/NiHCF-NPs/Zn/Fe-ZIF-NPC/GCE (B). Aptamer concentration: 2.0 μ M. Other modification conditions are the same as in Figure 3.

Moreover, the prepared AuNPs/NiHCF-NPs/Zn/Fe-ZIF-NPC/GCE were characterized using the CV technique. Firstly, the CV curves of AuNPs/NiHCF-NPs/Zn/Fe-ZIF-NPC/GCE at different scan rates were recorded. As shown in Figure 5A, higher current signals are obtained at higher scan rates and there is a good linear relationship between peak current and scan rate (inset of Figure 5A), corresponding to equations $I_{pa} (\mu A) = 83.41v (V s^{-1}) + 689.06 (R^2 = 0.994)$ and $I_{pc} (\mu A) = -60.37v (V s^{-1}) - 568.43 (R^2 = 0.992)$. The above phenomena indicate that the electrochemical reaction that occurred on the GCE was an adsorption-controlled process. Then, the prepared AuNPs/NiHCF-NPs/Zn/Fe-ZIF-NPC/GCE were placed in 0.1 M PBS and 30 consecutive cyclic voltammetric scans were conducted. The results obtained are shown in Figure 5B. It can be noticed that the CV curves were stable and the peak current remained at 93% of the initial value after 30 cycles, demonstrating the good stability of the constructed modified GCEs.

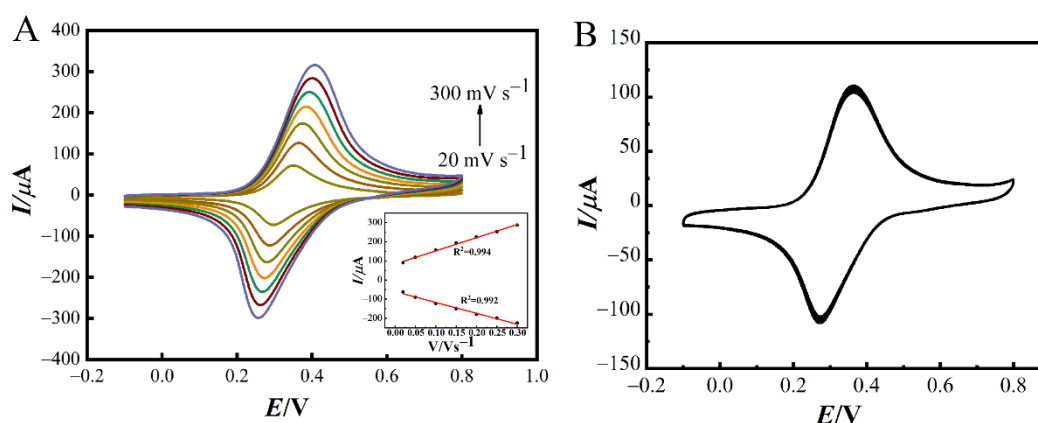


Figure 5. (A) CV curves of AuNPs/NiHCF-NPs/Zn/Fe-ZIF-NPC/GCE in 0.1 M PBS at various scan rates (from the inside to out: 0.02, 0.05, 0.10, 0.15, 0.20, 0.25 and 0.30 V s^{-1}), (Inset: the relationship between the peak current and scan rate), (B) CV curves of AuNPs/NiHCF-NPs/Zn/Fe-ZIF-NPC/GCE in 0.1 M PBS at 0.05 V s^{-1} . The modification conditions are the same as in Figure 3.

3.3. Electrochemical Behaviors of Different GCEs

Firstly, the electrochemical behavior of different modified GCEs during the aptasensor preparation processes was investigated by CV in 0.1 M PBS (pH = 7.0). As shown in Figure 6A,B, no redox peak appeared on bare GCE (curve g). However, a pair of distinct redox peaks appeared on NiHCF-NPs/GCE (curve a) with the oxidation peak current (I_{pa}) and reduction peak current (I_{pc}) of 10.89 μA and 6.65 μA . This pair of redox peaks was caused by the electron transfer between Fe^{3+} and Fe^{2+} in NiHCF-NPs [32]. After modification with Zn/Fe-ZIF-NPC (curve b), the I_{pa} and I_{pc} on NiHCF-NPs/Zn/Fe-ZIF-NPC/GCE increased to 33.42 μA and 28.62 μA , respectively, which were significantly higher than those on NiHCF-NPs/GCE, indicating that Zn/Fe-ZIF-NPC effectively enhanced the sensing signal, which was attributed to the promotion of electron transport by Zn/Fe-ZIF-NPC. After electrodeposition on AuNPs (curve c), I_{pa} and I_{pc} increased significantly to 95.86 μA and 87.29 μA , indicating that Au also has excellent electrocatalytic activity for the redox of NiHCF-NPs. Compared with NiHCF-NPs/GCE, the I_{pa} and I_{pc} signals generated by the NiHCF-NPs probe were 8.8-fold and 13.1-fold greater under the synergistic effect of Zn/Fe-ZIF-NPC and AuNPs, which would greatly improve the sensitivity of PQ detection. When Apt was self-assembled on the modified GCE through Au-S bonding [33], the I_{pa} and I_{pc} of Apt/AuNPs/NiHCF-NPs/Zn/Fe-ZIF-NPC/GCE (curve d) decreased to 60.85 μA and 45.18 μA . After blocking the unbound active site on the modified GCE surface with MCH [34], the I_{pa} and I_{pc} further decreased (curve e). Finally, after incubation of MCH/Apt/AuNPs/NiHCF-NPs/Zn/Fe-ZIF-NPC/GCE with PQ (10 mg/L) for 60 min, the I_{pa} and I_{pc} decreased once again (curve f), which was due to the formation of the PQ-Apt complex on the modified GCE surface impeding the electron transfer at the sensing interface. The above results combined with those in Figure 4 indicate that the aptasensor was successfully fabricated.

The interfacial properties of different GCEs were further characterized using EIS in 0.1 M KCl solution containing 5 mM $[\text{Fe}(\text{CN})_6]^{3-/4-}$ (1:1). As seen in Figure 7A,B, the R_{et} of bare GCE was approximately 692 Ω (curve a). After Zn/Fe-ZIF-NPC was modified, the R_{et} of Zn/Fe-ZIF-NPC/GCE decreased to 445 Ω (curve b). When NiHCF-NPs were further modified on Zn/Fe-ZIF-NPC/GCE, the R_{et} increased to 1784 Ω because the weak conductivity of NiHCF-NPs severely hindered the electron transfer between the GCE surface and the solution (curve d). However, compared to the R_{et} of 2712 Ω for NiHCF-NPs/GCE, the R_{et} of 1784 Ω for NiHCF-NPs/Zn/Fe-ZIF-NPC/GCE confirmed that Zn/Fe-ZIF-NPC can effectively facilitate electron transfer. After electrodeposition of AuNPs, the good conductivity of AuNPs reduced the R_{et} to 212 Ω (curve e). Subsequently, after aptamer and MCH were attached to the AuNPs/NiHCF-NPs/Zn/Fe-ZIF-NPC/GCE, the R_{et} increased to 1257

Ω (curve f) and 1680Ω (curve g) for Apt/AuNPs/NiHCF-NPs/Zn/Fe-ZIF-NPC/GCE and MCH/Apt/AuNPs/NiHCF-NPs/Zn/Fe-ZIF-NPC/GCE, respectively. This sharp increase of R_{et} can be explained by the electrostatic repulsion between the negatively charged phosphate backbone of Apt and the negative ions of $[\text{Fe}(\text{CN})_6]^{3-/4-}$ [35], and the non-conductive MCH hindered the electron-transfer. Finally, when the target molecule PQ was incorporated, the R_{et} further increased to 2536Ω (curve h), which was due to the non-conductive PQ-apramer complex hindering the electron transfer. The results of the EIS experiments were consistent with those of the CV experiments, again confirming the successful construction of the aptasensor.

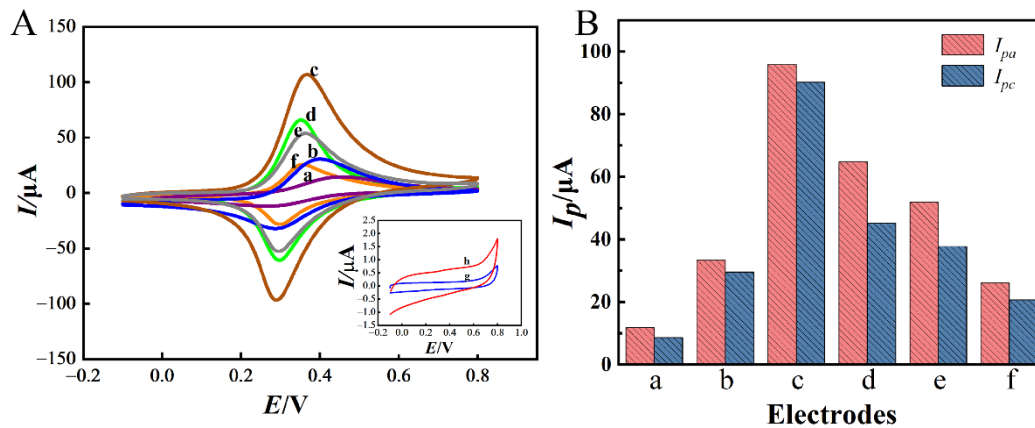


Figure 6. CV curves of different modified GCEs in 0.1 M PBS (pH = 7.0) (A) and the peak current values for different modified GCEs (B). a: NiHCF-NPs/GCE, b: NiHCF-NPs/Zn/Fe-ZIF-NPC/GCE, c: AuNPs/NiHCF-NPs/Zn/Fe-ZIF-NPC/GCE, d: Apt/AuNPs/NiHCF-NPs/Zn/Fe-ZIF-NPC/GCE, e: MCH/Apt/AuNPs/NiHCF-NPs/Zn/Fe-ZIF-NPC/GCE, f: PQ/MCH/Apt/AuNPs/NiHCF-NPs/Zn/Fe-ZIF-NPC/GCE, g: bare GCE, h: MCH/Apt/AuNPs/Zn/Fe-ZIF-NPC/GCE. The modification conditions are the same as in Figure 4.

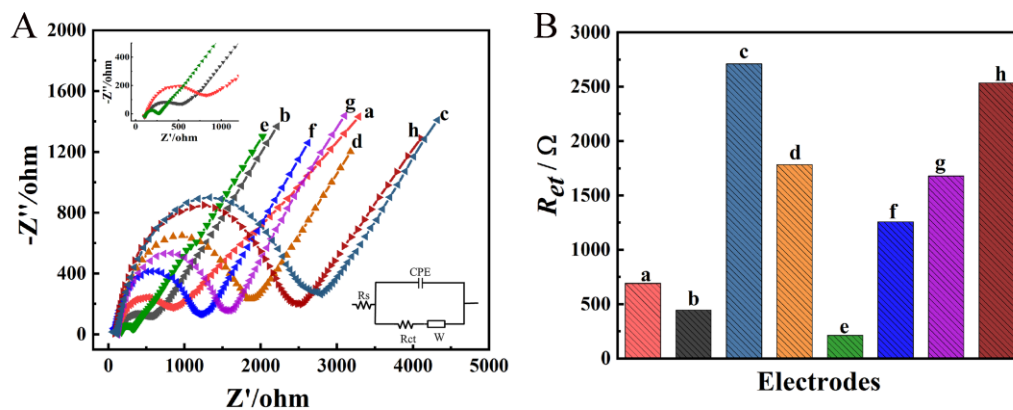


Figure 7. EIS of different modified GCEs in 0.1 M KCl solution containing the 5 mM $[\text{Fe}(\text{CN})_6]^{3-/4-}$ (1:1) (A) and the R_{et} values for different modified GCEs (B). a: bare GCE, b: Zn/Fe-ZIF-NPC/GCE, c: NiHCF-NPs/GCE, d: NiHCF-NPs/Zn/Fe-ZIF-NPC/GCE, e: AuNPs/NiHCF-NPs/Zn/Fe-ZIF-NPC/GCE, f: Apt/AuNPs/NiHCF-NPs/Zn/Fe-ZIF-NPC/GCE, g: MCH/Apt/AuNPs/NiHCF-NPs/Zn/Fe-ZIF-NPC/GCE, h: PQ/MCH/Apt/AuNPs/NiHCF-NPs/Zn/Fe-ZIF-NPC/GCE. The modification conditions are the same as in Figure 4.

3.4. Optimization of Experimental Parameters

In order to obtain the best sensing performance, the experimental parameters were optimized using the DPV technique.

First, the amount of Zn/Fe-ZIF-NPC was optimized (Figure 8A). When the loading volume of Zn/Fe-ZIF-NPC was increased from 4 μL to 8 μL , the current signal increased

and reached a maximum at 8 μL , then decreased. This is probably due to the fact that when the loading volume of Zn/Fe-ZIF-NPC was $\leq 8 \mu\text{L}$, a homogeneous film could be formed on the GCE surface and the electron transfer was promoted by Zn/Fe-ZIF-NPC. However, when the loading volume was higher than 8 μL , excessive loading would lead to the aggregation and accumulation of Zn/Fe-ZIF-NPC, which would instead be detrimental to electron transfer. Therefore, 8 μL was chosen as the optimal loading volume for Zn/Fe-ZIF-NPC.

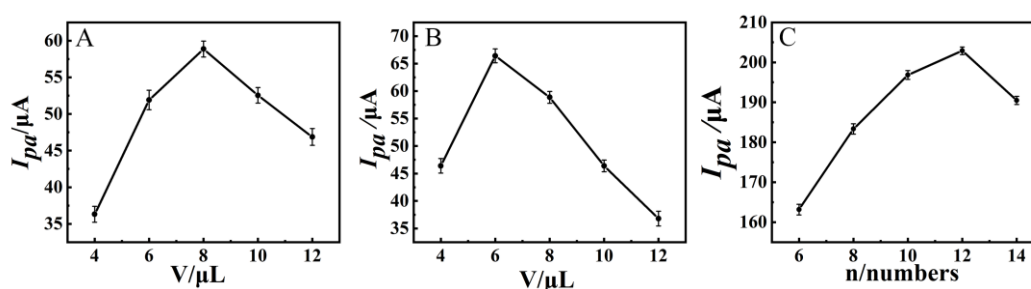


Figure 8. (A) Effect of Zn/Fe-ZIF-NPC loading volume on I_{pa} of NiHCF-NPs/Zn/Fe-ZIF-NPC/GCE, (B) Effect of NiHCF-NPs loading volume on I_{pa} of NiHCF-NPs/Zn/Fe-ZIF-NPC/GCE, (C) Effect of CV cycle numbers of AuNPs electrodeposition on the I_{pa} of AuNPs/NiHCF-NPs/Zn/Fe-ZIF-NPC/GCE. Error bars were obtained as the standard deviation of triple measurements ($n = 3$).

As the signal probe, NiHCF-NPs has a crucial influence on the analytical performance. The impact of NiHCF-NPs amount on the current signal is shown in Figure 8B; with the increase of NiHCF-NPs amount, the current signal first rose and then decreased, and the maximum current signal value was obtained at 6 μL . On the one hand, the more NiHCF-NPs contain more $\text{Fe}^{3+}/\text{Fe}^{2+}$ pairs, which can produce a larger sensing signal. On the other hand, NiHCF-NPs are less conductive, and more NiHCF-NPs impede electron transfer more, which can reduce the sensing signal. The combination of these two aspects resulted in an optimum loading volume of 6 μL .

Furthermore, the amount of AuNPs affects not only the sensing signal, but also the loading amount of aptamer. Within a certain range, the more AuNPs, the greater the sensing signal and the more active sites are available for binding the aptamer. However, too many AuNPs not only do not increase the number of binding sites for the aptamer but also make the sensing signal lower. In the electrodeposition process, the effect of CV scan number on the current signal is shown in Figure 8C. The current signal became larger as the number of cycles increased, and reached the maximum at 12 cycles. Thereafter, the current signal decreased. This is because too many cycles will cause the gold film to be too thick and block the electron transfer. Therefore, the number of CV cycles for depositing AuNPs was chosen to be 12.

The immobilization time and concentration of the aptamer were optimized and the results are presented in Figure 9. It can be seen that the I_p decreased with increasing immobilization time and remained almost constant after 12 h (Figure 9A). Hence, the immobilization time of 12 h was selected. In the range of $0.5\sim 3.5 \mu\text{mol L}^{-1}$, the I_{pa} also decreased with increasing concentration and tended to be stable when the concentration exceeded $2.5 \mu\text{mol L}^{-1}$ (Figure 9B), indicating that the binding of aptamer on the modified GCE surface reached saturation. Therefore, an aptamer of $2.5 \mu\text{mol L}^{-1}$ was selected for the preparation of the sensor. In addition, the effect of incubation time of PQ (10 mg/L) on the sensing performance was also investigated using percentage drop in current signal (ΦI) after incubation as the indicator (Figure 9C). It can be seen that as the incubation time was increased from 20 to 60 min, ΦI increased, indicating that more PQ was bound to the modified GCE. After 60 min of incubation, ΦI was almost unchanged, indicating that the binding between PQ and aptamer reached equilibrium. Therefore, the incubation time was chosen to be 60 min.

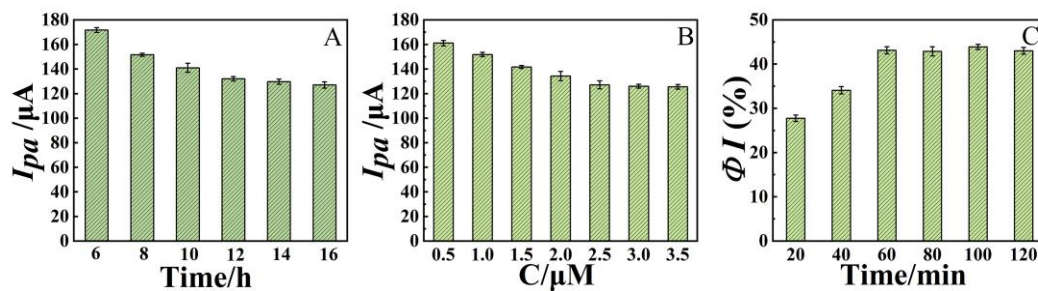


Figure 9. (A) Effects of immobilization time of aptamer on I_{pa} , (B) Effects of aptamer concentration on I_{pa} , (C) Effects of PQ incubation time on ΦI . Error bars were obtained as the standard deviation of triple measurements ($n = 3$).

3.5. Analytical Performance of the Proposed Aptasensor

DPV experiments were carried out to assess the analytical performance of the proposed aptasensor towards PQ. The DPV curves obtained are displayed in Figure 10A. It was observed that the current response of DPV gradually decreased with an increase in PQ concentration, which was attributed to the hindrance of electron transfer caused by PQ-aptamer complex formed on the aptasensor surface. Within the range of 0.001 mg/L to 100 mg/L, the ΦI versus $\log C_{\text{paraquat}}$ calibration plot is shown in Figure 10B. The regression equation was $\Phi I (\%) = 8.806 \times \log C + 33.134$ ($R^2 = 0.996$). The LOD was estimated to be 0.34 $\mu g/L$ based on $LOD = 3S_b/n$, where S_b is the SD of the blank solution and n is the slope of the calibration plot.

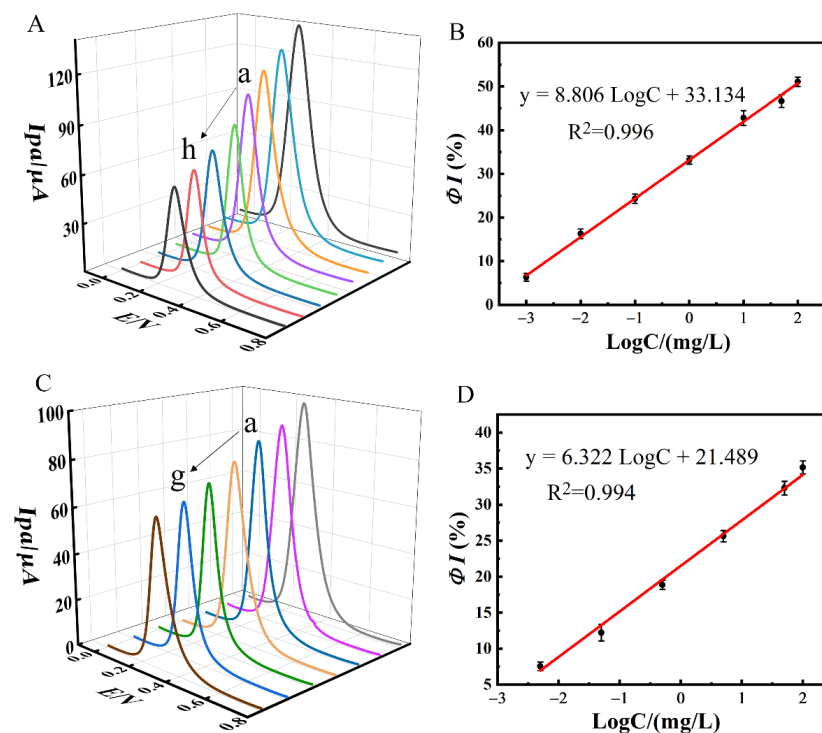


Figure 10. (A) DPV responses of MCH/Apt/AuNPs/NiHCF-NPs/Zn/Fe-ZIF-NPC/GCE in 0.1 M PBS at pH 7.0 after incubation with different concentrations of PQ (from a to h: 0, 0.001, 0.01, 0.1, 1.0, 10, 50, 100 mg/L), (B) the calibration curve for PQ detecting on MCH/Apt/AuNPs/NiHCF-NPs/Zn/Fe-ZIF-NPC/GCE. (C) DPV responses of MCH/Apt/AuNPs/NiHCF-NPs/GCE after incubation with different concentrations of PQ (from a to g: 0, 0.005, 0.05, 0.5, 5.0, 50, 100 mg/L), (D) the calibration curve for PQ detecting on MCH/Apt/AuNPs/NiHCF-NPs/GCE. Error bars were obtained as the standard deviation of triple measurements ($n = 3$).

As a comparison, the aptasensor without Zn/Fe-ZIF-NPC modification was also applied to detect PQ and the results are shown in Figure 10C,D. Again, ΦI (%) increased with increasing PQ concentration and the regression equation was ΦI (%) = 6.322 logC + 21.489 ($R^2 = 0.994$) over the range of 0.005–100 mg/L with an LOD of 2.29 $\mu\text{g/L}$. It can be noticed that compared to MCH/Apt/AuNPs/NiHCF-NPs/GCE, MCH/Apt/AuNPs/NiHCF-NPs/Zn/Fe-ZIF-NPC/GCE showed higher response sensitivity and lower LOD, which was attributed to the electrocatalytic effect of Zn/Fe-ZIF-NPC on the redox reaction of NiHCF-NPs which effectively improved the sensing signal.

Further, the test performance of the proposed aptasensor was compared with other PQ detection methods including electrochemical or non-electrochemical methods (Table 1). It can be found that the aptasensor proposed in this work has the lowest LOD and wider linear range. Moreover, the proposed aptasensor has the advantages of simplicity, low cost and good stability.

Table 1. Comparison of the proposed aptasensor with other PQ detection methods.

Technique	Methods *	Linear Range ($\mu\text{g L}^{-1}$)	LOD ($\mu\text{g L}^{-1}$)	Ref.
Electrochemistry	Paper-based silver sensor	558.9~1.863 $\times 10^4$	149.04	[36]
	Nf/SPGE(gel-based electrolyte platform)	186.3~1.12 $\times 10^4$	57.75	[37]
	BN/MoS ₂ /AuNPs/GCE	0~1.863 $\times 10^4$	13.79	[38]
	LMGCE	9.315~111.78	0.41	[39]
	CCDs/GCE	18.63~1863	11.92	[40]
	rGO-AB4	137.86~1829.47	4.30	[41]
	GC/MoS ₂ /CB [8]-DNPs	136~1490.4	40.99	[42]
	PtNPs@MIP/SPGrE	9.315~1.863 $\times 10^5$	3.73	[31]
Others	fluorescent sensors	5.0~350	1.20	[7]
	SERS	2.7~2.7 $\times 10^4$	2.70	[43]
	Colorimetric detection	9.315~93.15	4.69	[22]
	Colorimetric detection	0~5120	267.00	[27]
	Colorimetric detection	60~200	16.50	[28]
	SALDI-TOF MS	2~300	0.50	[44]
HPLC	0.1~1000	20.00	[45]	
	Apt/AuNPs/NiHCF-NPs/Zn/Fe-ZIF-NPC/GCE	1.0~1.0 $\times 10^5$	0.34	This work

* NF, nafion; SPGE, screen-printed graphene electrode; BN, boron nitride; GCE, glassy carbon electrode; LMGCE, phospholipid modified electrode; CCDs, carboxylatopillar[5]arene-coated nitrogen-doped carbon dots; rGO, reduced graphene oxide; AB4, activated biochar; GC, Glassy Carbon; CB [8], cucurbit[8]uril; DNPs, diamond nanoparticles; MIP, molecularly imprinted polymer; SPGrE, screen-printed graphene paste electrode; SERS, Surface enhanced Raman spectroscopy; SALDI-TOF MS, Surface-assisted laser desorption/ionization time-of-flight mass spectrometry; HPLC, high-performance liquid-chromatography.

The proposed sensor is more suitable for use in the lab. To achieve in situ detection of PQ, a combination of the proposed method with disposable electrodes (e.g., SPE) is needed, which is the content of our following research.

3.6. Reproducibility, Stability and Selectivity

The reproducibility of the proposed aptasensor was assessed. Seven independent sensors were used to detect PQ (10 mg/L) individually. The results showed that ΦI was very stable with an RSD of only 2.07%, indicating that the developed aptasensor has good reproducibility.

Storage stability is an important performance indicator for the sensor. The stability of the prepared aptasensor was examined from two aspects. The same batch of sensors was prepared and stored at 4 °C when not in use. Firstly, three sensors were taken and

their current response in 0.1 M PBS was measured periodically. The current response remained at 93% of the initial value after 28 days (Figure 11A), indicating that the modified materials and the NiHCF-NPs probes attached on the modified GCEs were stable during storage. Secondly, at intervals of 7 days, three fresh sensors were taken to measure their detection signal (ΦI) for the same concentration of PQ (10 mg/L) and it was observed that the ΦI value of the sensors was still 87.71% of the initial value after 28 days (Figure 11B), suggesting that the aptamer still maintained good bioactivity during the storage process. The above experimental results demonstrate good storage stability of the proposed sensor.

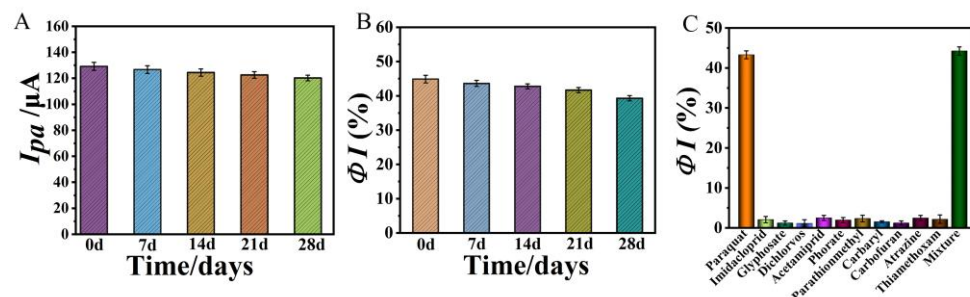


Figure 11. (A) Stability of the proposed aptasensor in 0.1 M PBS, (B) Stability of the proposed aptasensor for detection of PQ (10 mg/L), (C) Selectivity of the proposed aptasensor for PQ detection. Error bars were obtained as the standard deviation of triple measurements ($n = 3$).

To evaluate the selectivity of the as-prepared aptasensor for PQ detection, a series of pesticides including methomyl, acetamiprid, imidacloprid, dichlorvos, glyphosate, methyl parathion, thiamethoxam, carbofuran, atrazine and carbaryl were selected as interferents. According to the results shown in Figure 11C, there was no significant change in the current response when 10 mg/L of the other pesticides were used instead of 10 mg/L of PQ to incubate with the aptasensor. Meanwhile, when a mixture of 10 mg/L PQ and 10 mg/L other pesticides was incubated with the aptamer sensor, the current response changed significantly and the ΦI value was approximately equal to the value of 10 mg/L PQ only, indicating that the as-prepared aptasensor has excellent selectivity for PQ detection, which can be attributed to the specific recognition and affinity effect of the aptamer towards its target molecule.

3.7. Detection of PQ in Actual Samples

To verify the viability of the electrochemical aptasensor in practical application, the aptasensor was used for the detection of PQ in lettuce, cabbage and agriculture irrigating water samples. Since PQ was not detected in the original samples, different concentrations of PQ were added into the prepared samples for standard recovery experiments, and each concentration was detected three times in parallel. The recoveries measured were in the range of 96.20% to 104.02% with low RSD as shown in Table 2. This demonstrates the promising application of the constructed electrochemical aptasensor in the detection of PQ.

Table 2. Detection of PQ in real samples.

Samples	Added (mg/L)	Found (mg/L)	Recoveries (%)	RSD % ($n = 3$)
Water	0.01	0.0104 ± 0.0015	104.02	1.45
	1	0.9852 ± 0.03	98.52	3.32
	10	9.6450 ± 0.18	96.45	1.86
Lettuce	0.01	0.0102 ± 0.0004	102.43	4.35
	1	0.9620 ± 0.027	96.20	2.86
	10	10.3490 ± 0.386	103.49	3.73
Cabbage	0.01	0.0098 ± 0.0004	98.32	3.82
	1	1.0335 ± 0.035	103.35	3.40
	10	9.7790 ± 0.26	97.79	2.72

The possible matrix effects were investigated using the relative response value method and the results are shown in Figure 12. As seen in Figure 12A–C, the proposed sensors showed almost no change in DPV responses after incubation with the original actual samples. Subsequently, after incubation of the sensors with pure water containing 1 mg/L PQ and the actual samples containing 1 mg/L PQ for 60 min, respectively, the current drop percentage (ΦI (%)) was measured and the matrix effect was estimated according to $ME = A/B$, where A is the ΦI % caused by PQ in pure water matrix and B is the ΦI % caused by the same level of PQ in real sample matrix. It can be seen that the ME was between 98.98–101.73% (Figure 12D). The above results shows that the matrix effect is negligible.

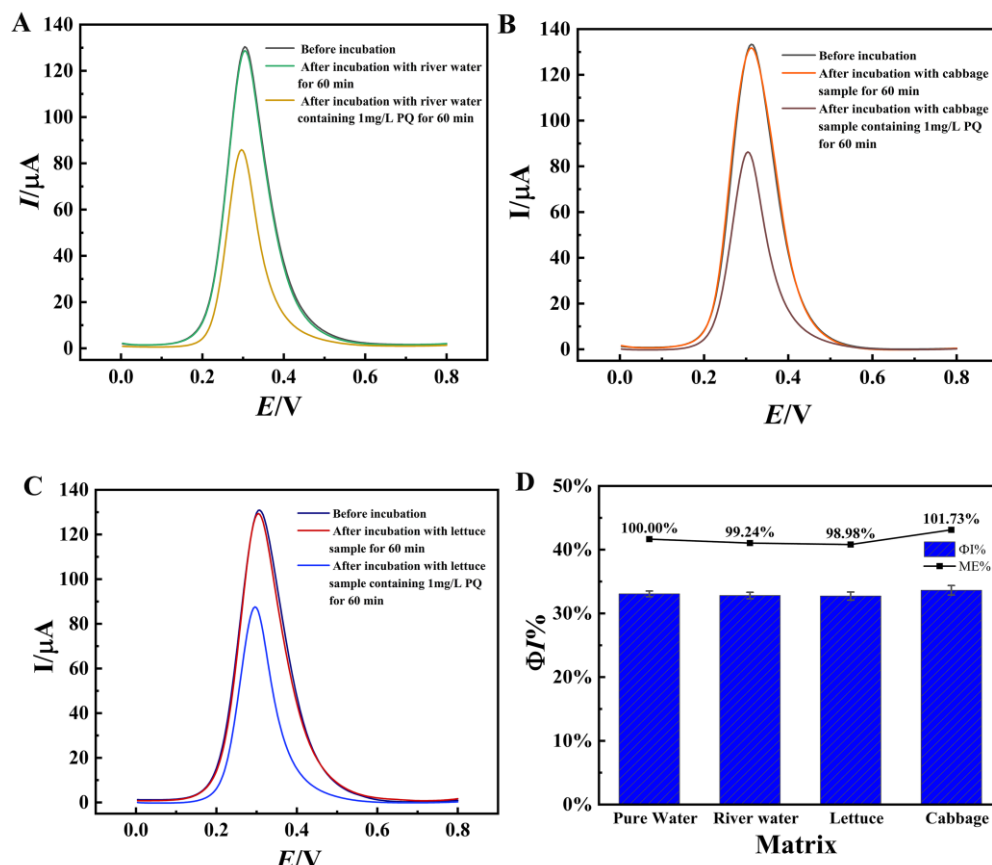


Figure 12. DPV curves of the aptasensors before and after incubation with different actual samples. (A) river water sample, (B) Cabbage sample, (C) lettuce sample and (D) ΦI % and ME values of the sensors after incubation with actual samples containing 1 mg/L PQ. Error bars were obtained as the standard deviation of triple measurements ($n = 3$).

4. Conclusions

In this work, a simple label-free electrochemical aptasensor was developed for the selective detection of PQ using NiHCF-NPs as the signal probe. Zn/Fe-ZIF-NPC has large specific surface area and porosity, and effectively accelerated the transfer of electrons. AuNPs also have high electrical conductivity. Based on the dual signal amplification effect of Zn/Fe-ZIF-NPC and AuNPs, highly sensitive detection of ultra-trace PQ was readily achieved with an LOD of 0.34 $\mu\text{g/L}$ and a wide linear range from 0.001 to 100 mg/L. The analysis results of PQ in real vegetable and agriculture irrigating water samples are satisfactory with satisfactory recoveries and low RSD, which proves that the proposed method is highly reliable and practical. Moreover, the sample pre-treatment and electrochemical detection operations of the proposed method are very simple. Therefore, the developed electrochemical aptasensor has the potential to be used as an advanced monitoring tool for the selective and highly sensitive assay of trace PQ residues in vegetable samples.

Author Contributions: Q.W.: Data curation, Methodology, Investigation, Formal analysis, Writing original draft, Validation. H.T.: Funding acquisition, Project administration, Data curation, Formal analysis, Methodology, Conceptualization, Supervision, Writing—review and editing. Y.W.: Funding acquisition, Formal analysis, Supervision. X.W.: Methodology, Investigation, Formal analysis. Q.S.: Investigation, Formal analysis, Validation. D.X.: Investigation, Formal analysis. All authors have read and agreed to the published version of the manuscript.

Funding: This work was financially supported by Guizhou Provincial Science and Technology Project (QKHJC-ZK [2022]Key015), the National Natural Science Foundation of China (32160603).

Institutional Review Board Statement: Not applicable.

Informed Consent Statement: Not applicable.

Data Availability Statement: The data presented in this study are available on request from the corresponding author.

Conflicts of Interest: There are no conflicts of interest to declare.

References

1. Jiang, Y.; Li, Q.; Yao, J.; Guo, X.; Ying, Y.; Liu, X.; Wen, Y.; Yang, H.; Wu, Y. Advanced photoelectrochemical detection of paraquat based on plasmonic metal modified photocathode material. *Appl. Surf. Sci.* **2022**, *581*, 151903. [[CrossRef](#)]
2. Dinis-Oliveira, R.J.; Duarte, J.A.; Sánchez-Navarro, A.; Remião, F.; Bastos, M.L.; Carvalho, F. Paraquat poisonings: Mechanisms of lung toxicity, clinical features, and treatment. *Crit. Rev. Toxicol.* **2008**, *38*, 13–71. [[CrossRef](#)] [[PubMed](#)]
3. Chen, J.; Su, Y.; Lin, F.; Iqbal, M.; Mehmood, K.; Zhang, H.; Shi, D. Effect of paraquat on cytotoxicity involved in oxidative stress and inflammatory reaction: A review of mechanisms and ecological implications. *Ecotox. Environ. Safe.* **2021**, *224*, 112711. [[CrossRef](#)] [[PubMed](#)]
4. Riahi, B.; Rafatpanah, H.; Mahmoudi, M.; Memar, B.; Brook, A.; Tabasi, N.; Karimi, G. Immunotoxicity of paraquat after subacute exposure to mice. *Food Chem. Toxicol.* **2010**, *48*, 1627–1631. [[CrossRef](#)] [[PubMed](#)]
5. Farahi, A.; Achak, M.; El Gaini, L.; El Mhammedi, M.A.; Bakasse, M. Electrochemical determination of paraquat in citric fruit based on electrodeposition of silver particles onto carbon paste electrode. *J. Food Drug Anal.* **2015**, *23*, 463–471. [[CrossRef](#)] [[PubMed](#)]
6. Laghrib, F.; Bakasse, M.; Lahrich, S.; El Mhammedi, M.A. Electrochemical sensors for improved detection of paraquat in food samples: A review. *Mat. Sci. Eng. C-Mater.* **2020**, *107*, 110349.1–110349.9. [[CrossRef](#)]
7. Ren, H.; Mao, M.; Li, M.; Zhang, C.; Peng, C.; Xu, J.; Wei, X. A Fluorescent Detection for Paraquat Based on β -CDs-Enhanced Fluorescent Gold Nanoclusters. *Foods* **2021**, *10*, 1178. [[CrossRef](#)]
8. Valera, E.; García-Febrero, R.; Pividori, I.; Sánchez-Baeza, F.; Marco, M.P. Coulombimetric immunosensor for paraquat based on electrochemical nanopores. *Sens. Actuators B Chem.* **2014**, *194*, 353–360. [[CrossRef](#)]
9. Kongpreecha, P.; Siri, S. Simple colorimetric screening of paraquat residue in vegetables evaluated by localized surface plasmon resonance of gold nanoparticles. *Biotechnol. Appl. Bioc.* **2022**, *69*, 1148–1158. [[CrossRef](#)]
10. Osman, K.A.; Al-Humaid, A.M.; Al-Rehiyani, S.M.; Al-Redhaiman, K.N. Monitoring of pesticide residues in vegetables marketed in Al-Qassim region, Saudi Arabia. *Ecotox. Environ. Safe.* **2010**, *73*, 1433–1439. [[CrossRef](#)]
11. Akhtar, S.; Yaqub, G.; Hamid, A.; Afzal, Z.; Asghar, S. Determination of Pesticide Residues in Selected Vegetables and Fruits from A Local Market of Lahore, Pakistan. *Curr. World Environ.* **2018**, *13*, 242–250. [[CrossRef](#)]
12. Sha, O.; Cui, B.; Chen, X.; Liu, H.; Yao, J.; Zhu, Y. Separation and Determination of Paraquat and Diquat in Human Plasma and Urine by Magnetic Dispersive Solid Phase Extraction Coupled with High-Performance Liquid Chromatography. *J. Anal. Methods Chem.* **2020**, *2020*, 7359582. [[CrossRef](#)] [[PubMed](#)]
13. Fu, Y.; Dai, X.; Fan, C.; Zheng, Y.; Fang, S.; Lin, Y.; Yi, Y.; Liao, L. A gas chromatography–Mass spectrometry-based metabonomic study on estimation of toxicant in rats. *J. Forensic Sci. Med.* **2019**, *5*, 80–86. [[CrossRef](#)]
14. Hui, F.; Xin, Z.; Shang, J.Z.; Luo, L.; Yong, M.Z.; Hai, J.X. Ultrasensitive and quantitative detection of paraquat on fruits skins via surface-enhanced Raman spectroscopy. *Sens. Actuators B Chem.* **2015**, *213*, 452–456. [[CrossRef](#)]
15. Wong, A.D.M.; Santos, A.M.; Cardenas-Riojas, A.A.; Baena-Moncada, A.M.; Sotomayor, M. Voltammetric sensor based on glassy carbon electrode modified with hierarchical porous carbon, silver sulfide nanoparticles and fullerene for electrochemical monitoring of nitrite in food samples. *Food Chem.* **2022**, *383*, 132384. [[CrossRef](#)]
16. Karimi-Maleh, H.; Beitollahi, H.; Kumar, P.S.; Tajik, S.; Jahani, P.M.; Karimi, F.; Karaman, C.; Vasseghian, Y.; Baghayeri, M.; Rouhi, J.; et al. Recent advances in carbon nanomaterials-based electrochemical sensors for food azo dyes detection. *Food Chem. Toxicol.* **2022**, *164*, 112961. [[CrossRef](#)] [[PubMed](#)]
17. Kong, F.Y.; Li, R.F.; Yao, L.; Wang, Z.X.; Li, H.Y.; Wang, W.J.; Wang, W. A novel electrochemical sensor based on Au nanoparticles/8-aminoquinoline functionalized graphene oxide nanocomposite for paraquat detection. *Nanotechnology* **2019**, *30*, 285502. [[CrossRef](#)]
18. Tan, X.; Zhang, Z.; Cao, T.; Zeng, W.; Huang, T.; Zhao, G. Control Assembly of Pillar [6]arene-Modified Ag Nanoparticles on Covalent Organic Framework Surface for Enhanced Sensing Performance toward Paraquat. *ACS Sustain. Chem. Eng.* **2019**, *7*, 20051–20059. [[CrossRef](#)]

19. Sohoul, E.; Ghalkhani, M.; Zargar, T.; Joseph, Y.; Rahimi-Nasrabadi, M.; Ahmadi, F.; Plonska-Brzezinska, M.E.; Ehrlich, H. A new electrochemical aptasensor based on gold/nitrogen-doped carbon nano-onions for the detection of *Staphylococcus aureus*. *Electrochim. Acta* **2022**, *403*, 139633. [[CrossRef](#)]
20. Zhao, Q.; Zhang, G.; Lu, D.; Feng, K.; Shi, X. Ultra-sensitive detection of ampicillin via dual-enzyme mediated cascade-signal amplified aptasensor. *Microchem. J.* **2021**, *164*, 106082. [[CrossRef](#)]
21. Ghalkhani, M.; Sohoul, E.; Khaloo, S.S.; Vaziri, M.H. Architecting of an aptasensor for the staphylococcus aureus analysis by modification of the screen-printed carbon electrode with aptamer/Ag-Cs-Gr QDs/NTiO₂. *Chemosphere* **2022**, *293*, 133597. [[CrossRef](#)] [[PubMed](#)]
22. Ran, X.D.; Wu, Y.G. Screening Aptamers and Development of Colorimetric Detection Method of Paraquat Pesticide. *Chin. J. Anal. Chem.* **2019**, *47*, 567–575. [[CrossRef](#)]
23. Janjani, P.; Bhardwaj, U.; Gupta, R.; Singh, K.H. Bimetallic Mn/Fe MOF modified screen-printed electrodes for non-enzymatic electrochemical sensing of organophosphate. *Anal. Chim. Acta* **2022**, *1202*, 339676. [[CrossRef](#)] [[PubMed](#)]
24. Casanova, A.; Iniesta, J.; Gomisberenguer, A. Recent progress in the development of porous carbon-based electrodes for sensing applications. *Analyst* **2022**, *147*, 767–783. [[CrossRef](#)] [[PubMed](#)]
25. Fei, Y.; Xueting, B.; Mingxing, L.; Jie, M. Recent progress on metal-organic framework-derived porous carbon and its composite for pollutant adsorption from liquid phase. *Chem. Eng. J.* **2021**, *405*, 126960. [[CrossRef](#)]
26. Torad, N.L.; Li, Y.; Ishihara, S.; Ariga, K.; Kamachi, Y.; Lian, H.; Hamoudi, H.; Sakka, Y.; Chaikittisilp, W.; Wu, K.C.W.; et al. MOF-derived Nanoporous Carbon as Intracellular Drug Delivery Carriers. *Chem. Lett.* **2014**, *43*, 717–719. [[CrossRef](#)]
27. Kuitio, C.; Klangprapan, S.; Chingkiti, N.; Boonthavivudhi, S.; Choowongkamon, K. Aptasensor for paraquat detection by gold nanoparticle colorimetric method. *J. Environ. Sci. Health. Part. B Pestic. Food Contam. Agric. Wastes* **2021**, *56*, 370–377. [[CrossRef](#)]
28. Zeng, H.; Yang, H.; Tang, Y.; Niu, X.; Wu, Y. Aptamer-enhanced the Ag(I) ion-3,3',5,5'-tetramethylbenzidine catalytic system as a novel colorimetric biosensor for ultrasensitive and selective detection of paraquat. *Spectrochim. Acta Part A Mol. Biomol. Spectrosc.* **2022**, *280*, 121571. [[CrossRef](#)]
29. Ma, S.; Wang, X.; Duan, H.; Wang, J.; Zhan, H.; Zhang, Z. A nanoporous carbon derived from bimetallic organic-framework for magnetic solid-phase extraction of bisphenol analogs. *Talanta* **2019**, *202*, 479–485. [[CrossRef](#)]
30. Jing, H.; Ying, Z.; Ya-Qin, C.; Ya-Li, Y.; Ruo, Y. Novel electrochemical catalysis as signal amplified strategy for label-free detection of neuron-specific enolase. *Biosens. Bioelectron.* **2012**, *31*, 399–405. [[CrossRef](#)]
31. Somnet, K.; Thimoonnee, S.; Karuwan, C.; Kamsong, W.; Tuantranont, A.; Amatongchai, M. Ready-to-use paraquat sensor using a graphene-screen printed electrode modified with a molecularly imprinted polymer coating on a platinum core. *Analyst* **2021**, *146*, 6270–6280. [[CrossRef](#)] [[PubMed](#)]
32. Na, L.; Zhongjie, L.; Junhua, Y.; Jianguo, H.; Jigen, M.; Qixian, Z.; Li, N.; Jixia, S. Nickel hexacyanoferrate nanoparticles anchored to multiwalled carbon nanotubes with a grafted poly(4-vinylpyridine) linker for electrically switched ion exchange. *Electrochim. Acta* **2012**, *72*, 150–156. [[CrossRef](#)]
33. Ali, D.; Biresaw, D.A.; Giuseppe, C.; Bajramshahe, S.; Asma, M.; Pietro, I.; Akm, S.I.; Luisa, P.; Paolo, L. Flexible Screen Printed Aptasensor for Rapid Detection of Furaneol: A Comparison of CNTs and AgNPs Effect on Aptasensor Performance. *Nanomaterials* **2020**, *10*, 1167. [[CrossRef](#)]
34. Liu, F.; Geng, L.; Ye, F.; Zhao, S. MOF-derived MnO@C nanocomposite with bidirectional electrocatalytic ability as signal amplification for dual-signal electrochemical sensing of cancer biomarker. *Talanta* **2022**, *239*, 123150. [[CrossRef](#)] [[PubMed](#)]
35. Lifang, F.; Caiyun, Z.; Wenjun, Y.; Yujing, G.; Shaomin, S.; Chuan, D.; Yingpu, B. Design of a facile and label-free electrochemical aptasensor for detection of atrazine. *Talanta* **2019**, *201*, 156–164. [[CrossRef](#)]
36. Deroco, P.B.; Wachholz Junior, D.; Kubota, L.T. Silver Inkjet-Printed Electrode on Paper for Electrochemical Sensing of Paraquat. *Chemosensors* **2021**, *9*, 61. [[CrossRef](#)]
37. Kanokwan, C.; Chuleekorn, C.; Siangproh, W.; Chailapakul, O. A new ready-to-use gel-based electrolyte for paraquat sensor. *Sensor. Actuat. B-Chem.* **2020**, *315*, 128089. [[CrossRef](#)]
38. Zhang, J.; Lin, Z.; Qin, Y.; Li, Y.; Liu, X.; Li, Q.; Huang, H. Fabricated Electrochemical Sensory Platform Based on the Boron Nitride Ternary Nanocomposite Film Electrode for Paraquat Detection. *ACS Omega* **2019**, *4*, 18398–18404. [[CrossRef](#)]
39. Tomková, H.; Sokolová, R.; Opletal, T.; Kučerová, P.; Kučera, L.; Součková, J.; Skopalová, J.; Barták, P. Electrochemical sensor based on phospholipid modified glassy carbon electrode—determination of paraquat. *J. Electroanal. Chem.* **2018**, *821*, 33–39. [[CrossRef](#)]
40. Zhang, H.; Huang, K.; Ding, L.; Yang, J.; Yang, Y.; Liang, F. Electrochemical determination of paraquat using a glassy carbon electrode decorated with pillararene-coated nitrogen-doped carbon dots. *Chin. Chem. Lett.* **2022**, *33*, 1537–1540. [[CrossRef](#)]
41. Sant'Anna, M.V.S.; Silva, J.D.S.; Gevaerd, A.; Lima, L.S.; Monteiro, M.D.S.; Carregosa, I.S.C.; Wisniewski, A.; Marcolino-Junior, L.H.; Bergamini, M.F.; Sussuchi, E.M. Selective carbonaceous-based (nano)composite sensors for electrochemical determination of paraquat in food samples. *Food Chem.* **2022**, *373*, 131521. [[CrossRef](#)] [[PubMed](#)]
42. Blanco, E.; Rocha, L.; Pozo, M.D.; Vázquez, L.; Petit-Domínguez, M.D.; Casero, E.; Quintana, C. A supramolecular hybrid sensor based on cucurbit [8]uril, 2D-molibdenum disulphide and diamond nanoparticles towards methyl viologen analysis. *Anal. Chim. Acta* **2021**, *1182*, 338940. [[CrossRef](#)]
43. Raju, B.; Pitak, E.; Mati, H.; Saksorn, L.; Chanunthorn, C.; Viyapol, P.; Ryo, M.; Apichai, J.; Noppadon, N. 3D structured laser engraves decorated with gold nanoparticle SERS chips for paraquat herbicide detection in environments. *Sens. Actuators B Chem.* **2020**, *304*, 127327. [[CrossRef](#)]

44. Tan, W.; Xu, X.; Lv, Y.; Lei, W.; Hu, K.; Ye, F.; Zhao, S. Sulfonic acid functionalized hierarchical porous covalent organic frameworks as a SALDI-TOF MS matrix for effective extraction and detection of paraquat and diquat. *J. Colloid Interf. Sci.* **2021**, *603*, 172–181. [[CrossRef](#)] [[PubMed](#)]
45. Marzieh, R.; Rouhollah, H.; Afshin, M.; Ebrahim, M.; Behroz, D. Salt-assisted liquid–liquid extraction coupled with reversed-phase dispersive liquid–liquid microextraction for sensitive HPLC determination of paraquat in environmental and food samples. *J. Food Meas. Charact.* **2019**, *13*, 269–276. [[CrossRef](#)]